HHS Public Access

Author manuscript

Sci Signal. Author manuscript; available in PMC 2016 April 29.

Published in final edited form as:

Sci Signal. ; 9(422): ra35. doi:10.1126/scisignal.aad6281.

Defining the Stoichiometry of Inositol 1,4,5-Trisphosphate Binding Required to Initiate Ca^{2+} Release

Kamil J. Alzayady[1], **Liwei Wang**[1], **Rahul Chandrasekhar**[1], **Larry E. Wagner II**[1], **Filip Van Petegem**[2], and **David I. Yule**[1,*]

[1]Department of Pharmacology and Physiology, University of Rochester, Rochester NY 14642 USA

[2]Department of Biochemistry and Molecular Biology, University of British Columbia, Canada

Abstract

Inositol 1,4,5-trisphosphate (IP_3) receptors (IP_3Rs) are tetrameric intracellular Ca^{2+}-release channels with each subunit containing a binding site for IP_3 in the N-terminus. We provide evidence that four IP_3 molecules are required to activate the channel under diverse conditions. Comparing the concentration-response relationship for binding and Ca^{2+} release suggested that IP_3Rs are maximally occupied by IP_3 before substantial Ca^{2+} release occurs. We showed that ligand binding–deficient subunits acted in a dominant-negative manner when coexpressed with wild-type monomers in the chicken immune cell line DT40-3KO, which lacks all three genes encoding IP_3R subunits, and confirmed the same effect in an IP_3R-null human cell line (HEK-3KO) generated by CRISPR/Cas9 technology. Using dimeric and tetrameric concatenated IP_3Rs with increasing numbers of binding-deficient subunits, we addressed the obligate ligand stoichiometry. The concatenated IP_3Rs with four ligand-binding sites exhibited Ca^{2+} release and

*To whom correspondence should be addressed: David I. Yule, Department of Pharmacology and Physiology, 601 Elmwood Avenue, Rochester, NY 14642. Tel: 585 273 2154. david_Yule@urmc.rochester.edu.

Author Contributions: K.J.A, L. W., R.C, and L. E. W.II, performed research and analyzed data. F. L.A. V. P. performed homology modeling. D.I.Y. conceived and supervised the project and analyzed data. K.J.A, L. E. W. II, F. L.A. V. P. and D.I.Y. wrote the paper. All authors read and approved the final manuscript.

Competing interests: The authors declare that they have no completing interests.

Data and materials availability: Constructs and cell lines will be made freely available for academic use following completion of a Material Transfer Agreement (MTA) between the University of Rochester and requesting institution.

Supplemental Materials

Figure S1. Assessment of $R1_Q$ Ca^{2+} release activities in response to endothelin and BCR stimulation.
Figure S2. Generation of HEK293 cells with IP_3R-null background using CRISPR/Cas9 technology.
Figure S3. Ca^{2+} release activity of DT40-3KO cells expressing $R1R1_{QQQ}$ or $R1_{QQQ}R1$ in response to endothelin and BCR stimulation
Figure S4. Ca^{2+} release activity of IP_3R1 channel incorporating two $R1_Q$ subunits.
Figure S5. Ca^{2+} release activity of R1R1R1R1 in response to endothelin and BCR stimulation.
Figure S6. IP_3R1 channels assembled from concatenated IP_3R1 have identical single channel properties as that of wild type IP_3R1.
Figure S7. Modulation of single-channel properties of concatenated IP_3R1 by ATP
Figure S8. Modulation of single-channel properties of concatenated IP_3R1 by calcium.
Figure S9. Analysis of IP_3R burst kinetics.
Figure S10. Representative current amplitude histograms for IP_3R1 activity.
Figure S11. Assessment of $R1R1_{QQQ}R1R1_{QQQ}$ Ca^{2+} release activities in response to trypsin.
Figure S12. Ca^{2+} release activities of $R1R1R1R1_{QQQ}$ in response to endothelin and BCR stimulation.
Supplemental Table 1: Genomic analysis of HEK-3KO cells.
Supplemental Table 2: Biophysical Characteristics of IP_3R and Concatenated IP_3R. Constructs.
Supplemental Table 3: List of primers used in this study.

electrophysiological properties of native IP_3Rs. However, IP_3 failed to activate IP_3Rs assembled from concatenated dimers consisting of one binding-competent and one binding-deficient mutant subunit. Similarly, IP_3Rs containing two monomers of IP_3R2_{short}, an IP_3 binding-deficient splice variant, were nonfunctional. Concatenated tetramers containing only three binding competent ligand-binding sites were nonfunctional under a wide range of activating conditions. These data provide definitive evidence that IP_3-induced Ca^{2+} release only occurs when each IP_3R monomer within the tetramer is occupied by IP_3, thereby ensuring fidelity of Ca^{2+} release.

Introduction

The modulation of intracellular calcium concentration $[Ca^{2+}]_i$ is a signal used by all living organisms to control many cellular processes, including gene transcription, regulated secretion, proliferation, muscle contraction, fertilization, and apoptosis (1). Inositol 1,4,5-trisphosphate (IP_3) receptors (IP_3Rs) are ligand-gated calcium channels present in most eukaryotic species (1-3). There are three homologous isoforms ubiquitously distributed in mammalian tissues (denoted as IP_3R1, IP_3R2, and IP_3R3) (4). The individual channel is assembled with a tetrameric architecture consisting of homo- or heteromeric subunits and is localized in the membranes of intracellular calcium stores, such as the endoplasmic reticulum and sarcoplasmic reticulum (3, 5). Each IP_3R subunit is ~ 2700 amino acids and consists of three functional domains: the N-terminal IP_3-binding domain, an intervening modulatory domain, and the C-terminal channel domain containing six transmembrane helices and the Ca^{2+}-permeable pore (5, 6). All known regulatory sites, including phosphorylation sites, nucleotide-binding sites, and interaction motifs with protein binding partners are present in each monomer (3, 5, 7). Accordingly, each monomer contributes a ligand-binding site to the tetrameric channel.

Previous studies suggest that IP_3 binding triggers inter- or intramolecular conformational changes between subunits involving interactions between the N- and C-termini that ultimately culminate in channel opening and Ca^{2+} release (8-11). However, fundamental questions regarding the molecular basis of channel gating remain (12, 13). For example, the number of IP_3 molecules required to open the tetrameric IP_3R channel is not established; indeed, the stoichiometry necessary for any regulatory input is not known. Understanding the stoichiometry of IP_3R regulation is especially important, because IP_3R dysfunction as a result of mutations in the protein has been implicated in human pathologies, such as anhidrosis (an inability to perspire) and spinocerebellar ataxia (14-16), and IP_3R-associated diseases occur in the heterozygous condition in which the IP_3R channel is likely formed from various combinations of normal and mutant monomers (16, 17).

Although IP_3 binding to IP_3R is not generally reported to be highly cooperative (18, 19), some studies have reported Ca^{2+} release to be highly cooperative in permeabilized cell systems (20, 21). This cooperative relationship could be a consequence of Ca^{2+} facilitating further release by acting as a co-agonist; however, the cooperativity has been observed in experiments in which intracellular Ca^{2+} is buffered (20, 22). One explanation for the cooperative Ca^{2+} release has been that at least three ligand-binding events are required for channel opening (20, 23). Contrary to this idea, transiently expressed IP_3R channels

engineered with only two intact binding sites are reported to be activated by IP_3 (10). Further, structural analysis by cryo-electron microscopy (cryo-EM) suggests that, as a result of interactions between the C terminus of one subunit and the N termini of neighboring subunits, IP_3 binding to one subunit induces conformational changes in two adjacent subunits and, thus, this model implies the requirement for binding of less than 4 four molecules of IP_3 for channel gating (11). Nevertheless, a comprehensive molecular methodology has never been attempted to address how many IP_3 molecules are necessary to activate IP_3R channels. Here, we engineered concatenated IP_3R, in which progressive numbers of IP_3-binding sites were disrupted either by mutation or incorporation of naturally occurring binding-deficient mutants. Furthermore, we expressed these concatenated receptors in cells lacking IP_3Rs, thereby avoiding issues of incorporation of endogenous subunits into the channel. With these concatenated receptors, we systematically monitored IP_3R activity and addressed the stoichiometry of IP_3 molecules required for optimum channel function. Our data establish that IP_3-induced Ca^{2+} signals are only initiated following occupation of IP_3R by four IP_3 molecules.

Results

The relationship between IP_3 binding and IP_3R activation is complex

The DT40-3KO cell line is a chicken B-lymphoid cell type that has been genetically modified to be deficient in all subunits of the IP_3R (24, 25). Thus, these cells provide a system for analyzing IP_3Rs with controlled subunit composition. We investigated the relationship between IP_3 binding and IP_3-induced Ca^{2+} release by comparing data obtained from competitive ^3H-IP_3 binding assays and unidirectional Ca^{2+} release assays performed in permeabilized DT40-3KO cells expressing rat IP_3R1. Ca^{2+} release was only triggered following substantial (~82%) steady-state receptor occupancy (Fig. 1). By necessity, the ^3H-IP_3 binding and Ca^{2+} release assays were performed under somewhat different assay conditions including differences in the experimental buffers and assay endpoints. Despite this caveat, if extrapolated to dynamic conditions in intact cells responding to a natural IP_3-generating stimulus, the results are consistent with Ca^{2+} release only being activated at any particular IP_3 concentration ($[IP_3]$) when the probability is high that most, if not all, subunits are occupied by IP_3 at a given time (20). Thus, these data suggest that multiple subunits must be occupied to initiate Ca^{2+} release.

Next, we tested if incorporating IP_3 binding-defective subunit(s) into the tetrameric assembly impaired IP_3R channel function. Positively charged residues scattered in the N terminus of IP_3R subunits mediate IP_3 binding (26). These early studies, which defined the IP_3 binding domain, replaced key arginine and lysine residues absolutely required for IP_3 binding with glutamine. The rationale being that lysine, arginine, and glutamine are amphipathic and have similar side chain conformational entropy and, thus, the mutation, while negating the positive charge, is predicted to be less disruptive to the structural and functional integrity of the receptor (26). In mammalian IP_3R family members, there are ten conserved basic residues that are essential for binding and three of which are considered critical for specific binding (R^{265}, K^{508}, and R^{511}, residue numbering based on rat IP_3R1) (26). Although initial studies using IP_3R1 with a single R265Q mutation reported that this

mutant does not bind IP_3 and, thus, is not activated by IP_3 (10, 26), a subsequent study showed that this construct retains IP_3 binding capacity (27).

To resolve this discrepancy, we generated two different IP_3R1 mutants $IP_3R1.R265Q$ (designated as $R1_Q$) and $IP_3R1.R265/K508/R511Q$, (designated as $R1_{QQQ}$), and stably transfected plasmids encoding these into IP_3R null, DT40-3KO cells. When compared to wild-type IP_3R1 (designated as R1), $R1_{QQQ}$ retained no binding activity, whereas $R1_Q$ retained low, but detectable binding (~10%) (Fig. 2A). In permeabilized cell unidirectional Ca^{2+} release assays, IP_3 evoked robust Ca^{2+} release from cells expressing R1, but IP_3 failed to release Ca^{2+} in nontransfected DT40-3KO cells or cells stably expressing $R1_{QQQ}$ (Fig. 2B). However, cells expressing $R1_Q$ produced a small, but measurable, Ca^{2+} signal in response to exogenous IP_3, suggesting that the residual binding capacity of this mutant supported limited channel activation under these assay conditions.

Using the stably transfected DT40-3KO, we investigated the ability of these IP_3R1 constructs to respond to IP_3-generating stimuli in intact cells. We challenged cells with the $G\alpha_q$-coupled G protein-coupled receptor (GPCR) agonists, endothelin and trypsin. We also stimulated the B cell receptor (BCR), a tyrosine kinase receptor by crosslinking with anti IgM antibody. All three IP_3 producing stimuli failed to trigger Ca^{2+} release in DT40-3KO and cells expressing $R1_Q$ or $R1_{QQQ}$; whereas DT40-3KO cells expressing R1 showed robust responses to all three stimuli (Fig. 2C and D and fig. S1A and S1B). The contradictory behavior of $R1_Q$ in the two assay systems is likely due to the different experimental conditions. In particular, the permeabilized cell assay exposes IP_3R to uniform maximum concentrations of IP_3 and ATP; whereas the intact cell assay relies on endogenously produced IP_3 downstream of surface receptor signaling that likely results in less intense stimulation. These data clearly illustrated that the use of the single point mutation (R265Q) is inadequate for assessing ligand stoichiometry. Therefore, we used $R1_{QQQ}$ for the subsequent experiments.

Mutagenesis in the ligand-binding domain is unlikely to result in a global structural rearrangement of IP_3R

A concern associated with functional analysis of mutated proteins is that any substitution may interfere with protein folding, resulting in unwanted, allosteric effects beyond the intended targeted disruption. To investigate whether the introduction of glutamine residues in $R1_{QQQ}$ markedly disrupted the overall structural integrity of IP_3R1, we analyzed the available IP_3R structures. A cryo-EM study at 4.7Å shows the full-length IP_3R (Fig. 3A), but the local resolution in the IP_3-binding site is not sufficient to reveal individual side chains (11). Therefore, we used a crystal structure of the N-terminal region, captured in the absence of IP_3 (28). The crystal structure contains two IP_3R molecules in the asymmetric unit, which show identical folds and relative domain orientations upon superposition. Each of the three mutated residues (R^{265}, K^{508}, R^{511}) are surface accessible, and are not involved in domain-domain interactions (Fig. 3B and C). To verify that the mutations are sterically allowed, we generated a homology model of the ligand-binding domain using Modeller, which satisfied spatial restraints (29). Although a high-resolution structure of the $R1_{QQQ}$ mutant would be required to unequivocally rule out any major conformational changes, our

homology model predicted that the glutamine side chains did not produce substantial rearrangements of neighboring residues. Furthermore, the side chains of R^{265} and K^{508} make no significant interactions with other residues, and the few hydrogen bonds (Fig. 3C) are only observed in one out of two molecules in the asymmetric unit. R^{511} makes hydrogen bonds with two neighboring residues, observed in both molecules of the asymmetric unit (Fig. 3C). However, because these residues are within the same domain, we predict that it is unlikely that disruption would result in long-range allosteric effects (Fig. 3D). In conclusion, although conformational changes and allosteric effects of the $R1_{QQQ}$ mutant cannot be completely ruled out, we deem this unlikely.

$R1_{QQQ}$ subunits exert an apparent dominant-negative effect on IP_3R1 activity

We hypothesized that if incorporation of $R1_{QQQ}$ subunit(s) into tetrameric IP_3R attenuated IP_3-induced Ca^{2+} release, it would indicate a dominant-negative effect and suggest that full occupancy of IP_3R monomers with IP_3 is required to induce Ca^{2+} release. We transiently transfected wild-type IP_3R1 tagged with mCherry (cherryR1) or empty vector into DT40-3KO or DT40-3KO stably expressing a high level of $R1_{QQQ}$. We used the mCherry fusion construct to identify transfected cells. Because both transiently and stably transfected IP_3R1 constructs are driven by an exogenous CMV promoter, we anticipated that nascent subunits would oligomerize to form tetrameric IP_3R complexes in various combinations. To establish that transiently transfected R1 oligomerized with stably expressed R1 proteins in the DT40-3KO cell system, we performed coimmunoprecipitation experiments, which confirmed that transiently expressed cherryRl associated with stably expressed FLAG-tagged IP_3R1 (Fig. 4A, inset). Although we cannot formally exclude the possibility of intermolecular interactions between adjacent homomeric populations of IP_3R constructs, these data suggested that tetrameric IP_3R complexes can be assembled from transiently and stably co-expressed IP_3R subunits in DT40-3KO cells.

DT40-3KO transfected with cherryRl supported robust Ca^{2+} release in response to trypsin, whereas stimulation of $R1_{QQQ}$ cells transfected with cherryRl resulted in weak Ca^{2+} release (Fig. 4A and pooled data in B). These data indicated that, although transiently transfected cherryRl assembled to form functional channels in DT40-3KO, the co-expression and incorporation of ligand-binding defective subunit(s) inhibited the formation of competent channels. Taken together, these findings suggested that incorporating a mutant subunit(s) impairs the tetrameric channel function, which supports the hypothesis that an IP_3R with less than four intact ligand-binding sites does not function as an IP_3-gated Ca^{2+} channel.

Although DT40-3KO cells are a useful expression system, there are caveats associated with this cell line, such as their relatively low transfection efficiency and their non-mammalian origin. Therefore, we sought to confirm our findings in a mammalian cell type. Human embryonic kidney (HEK293) cells are widely used, easily maintained, and readily transfected, but all three IP_3R subtypes are present in these cells (fig. S2A). To generate IP_3R-null HEK293 cells, we used CRISPR/Cas9 gene editing to simultaneously disrupt all three IP_3R-encoding genes (30). Genotyping, Western blot analyses, and single-cell imaging confirmed the disruption of IP_3R-encoding genes and the absence of functional IP_3Rs (fig. 2A, S2B, and table S1).

We assessed the effect of wild-type IP_3R1 and binding-defective subunit ($R1_{QQQ}$) on channel function in these IP_3R-deficient HEK293 cells (designated as HEK-3KO). The amount of cherryRl was similar under both conditions (Fig. 4C, inset). As expected, cherryRl expressed alone mediated robust Ca^{2+} release in response to trypsin (Fig. 4C and pooled data in Fig. 4D). Co-expression of $R1_{QQQ}$ with cherryRl significantly attenuated the trypsin-induced Ca^{2+} response. Co-transfection would be anticipated to result in a binomial distribution of heterotetrameric assemblies of all combination of R1 and $R1_{QQQ}$ (31). The degree of inhibition of Ca^{2+} release appears inconsistent with a minority population of homomeric $R1_{QQQ}$ and indicates that the mutant subunit likely exhibits dominant-negative effects when present in the complex with some wild-type subunits.

IP_3R1 tetramers with two IP_3 binding-deficient subunits lack activity

Our results thus far indicated that a tetrameric channel with less than four intact binding sites is not an IP_3-gated Ca^{2+} channel. However, in these experimental paradigms, it is not possible to define accurately the subunit composition of each assembled channel. To address precisely how many binding sites are required for channel activation, we generated concatenated channels with predefined subunit composition. Constructs encoding dimeric concatenated IP_3R (for cartoon see Fig. 5A) generate proteins that dimerize to form authentic IP_3-gated tetrameric channels (Fig 5B) (32, 33). To determine if IP_3R channels with two ligand-binding deficient subunits are functional, we engineered concatenated IP_3R constructs in which two IP_3R1 molecules are linked tail-to-head. We constructed two dimeric concatenated receptors with different configurations containing wild-type subunits and IP_3-binding-deficient subunits, designated as $R1R1_{QQQ}$ and $R1_{QQQ}R1$, and stably expressed them in DT40-3KO (Fig. 6A). Permeabilized cell assays demonstrated that cells expressing $R1R1_{QQQ}$ did not produce any Ca^{2+} release in response to application of IP_3, suggesting that channels containing two mutant subunits were not functional (Fig. 6B). Furthermore, consistent with the dimeric binding-deficient constructs not forming functional channels, cells expressing either $R1R1_{QQQ}$ or $R1_{QQQ}R1$ did not produce a Ca^{2+} signal in response to trypsin (Fig. 6C and pooled data in D), endothelin, or BCR stimulation of intact cells (fig. S3A and S3B). Taken together, these findings showed that binding of two IP_3 molecules is not sufficient to activate tetrameric IP_3R channels. Of note, we observed Ca^{2+}-release activity in both the permeabilized cell assay and by single-cell imaging in cells expressing tetrameric channels assembled from R1qR1 or R1R1q dimers (fig. S4A-D). These channels consist of two wild-type IP_3R subunits and two $R1_Q$ subunits. The results are consistent with the residual binding activity of monomeric $R1_Q$ subunits (Fig. 2A).

A functional IP_3R1 channel can be generated as one concatenated molecule

To precisely control the subunit composition of the receptor without the complicating factor of oligomerization, we generated IP_3R from a single concatenated polypeptide with a 14-amino-acid linker between the subunits and expressed this protein in DT40-3KO cells. We confirmed by Western blotting that the wild-type version of this IP_3R1 construct (R1R1R1R1) could be stably expressed in DT40-3KO cells (Fig. 7A,-left). Cells expressing R1R1R1R1 exhibited robust IP_3-induced Ca^{2+} release in the permeabilized cell assay (Fig. 7B) and agonist-induced Ca^{2+} signals in intact cells (Fig. 7C-D) and (fig. S5A-B). Pivotal to interpretation of these data is to confirm that the concatenated tetrameric channel behaves in

an identical fashion to IP_3R assembled from wild-type subunits. To confirm that the concatenated channel generated from a single polypeptide chain had the same electrophysiological properties as IP_3R assembled from wild-type monomer subunits, we performed extensive electrophysiological analyses of single channel properties with the on-nucleus configuration of patch clamp. ATP and Ca^{2+} function as co-agonists with IP_3 of the IP_3R and enhance the responsiveness of the channel IP_3 (3, 34). Single-channel recordings of R1R1R1R1 showed that the channel was activated by IP_3 and that the response to IP_3 was enhanced by either increasing the concentration or ATP (Fig. 7E, left) or Ca^{2+} (Fig. 7E, right). Indeed, the activity of channels produced from monomers, concatenated dimers, or the single polypeptide concatenated tetramer were indistinguishable in terms of current-voltage relationship (fig. S6A-D), regulation by Ca^{2+} and ATP (fig. S7 and S8), and the biophysical characteristics of gating (fig. S9 and S10), all of which define IP_3R activity. Thus, channels formed from concatenated R1R1R1R1 have biophysical properties of native channels and function as bona fide IP_3Rs (Table 1 and table S2). We first used this concatenated single polypeptide approach to examine the response of cells expressing an IP_3R with only two IP_3-binding sites ($R1R1_{QQQ}R1R1_{QQQ}$). Consistent with data generated with the $R1R1_{QQQ}$ dimer-expressing cells, $R1R1_{QQQ}R1R1_{QQQ}$ expression did not support trypsin-stimulated Ca^{2+} signals (fig. S11).

IP_3R1 -with a single IP_3 binding-deficient subunit lack activity

Using the single concatenated polypeptide channel approach, we assessed if an IP_3R lacking only a single IP_3 binding-site was functional. We generated a single polypeptide construct containing three wild-type subunits conjugated to one $R1_{QQQ}$ subunit ($R1R1R1R1_{QQQ}$) and stably expressed this protein in DT40-3KO cells (Fig. 7A, right panel). Cells expressing this construct were unresponsive to application of IP_3 in the permeabilized cell assay (Fig. 7B) and did not display any Ca^{2+} signal in intact cells when stimulated with trypsin (Fig. 7C and pooled data in D) or endothelin (fig. S12A) or in response to BCR stimulation (fig. S12B). In single-channel electrophysiological studies, varying Ca^{2+} and ATP with IP_3 concentrations as high as 100 μM never elicited any IP_3R channel activity (Fig. 7F). In total, these data suggested that a fundamental property of the IP_3R is the requirement for each monomer to bind IP_3 to achieve channel activation.

IP_3R2 containing two binding-deficient $IP_3R2_{(short)}$ splice variant subunits lack activity

The necessity for IP_3 binding to each subunit of the IP_3R tetramer may also have physiological consequences beyond the fundamental biophysical requirement to initiate Ca^{2+} release. A widely distributed splice variant of mammalian IP_3R2 ($R2_{short}$) does not bind IP_3 despite having an intact ligand-binding domain (18). This splice variant lacks amino acids 176-208. These amino acids are in the region termed the “suppressor domain” which is a major modulator of IP_3 binding affinity (19, 26), and channels formed by this variant are nonfunctional (18). We determined by coimmunoprecipitation that this splice variant formed heteromeric channels when expressed in HEK-293 cells with other full-length isoforms (Fig. 8A), consistent with previous reports that indicate that transiently transfected IP_3Rs assemble into tetrameric complexes (31). IP_3 binding in permeabilized DT40-3KO cells expressing a dimer of $R2R2_{short}$ was reduced by ~50% when compared with dimeric R2R2 composed of wild-type IP_3R2 and comparable to binding to $R2R2_{QQ}$, a

construct with 2 amino acids mutations in IP_3R2 corresponding to amino acids analogous to those involved in IP_3 binding in IP_3R1 (Fig. 8B). However, a channel containing two subunits of $R2_{short}$ or $R2_{QQ}$ was not functional in response to trypsin activation (Fig. 8C and pooled data in D). These results indicated that this widely distributed variant could incorporate into tetrameric receptors and that the result would be to dampen or even eliminate intracellular Ca^{2+} signals produced by IP_3-stimulated release from the intracellular stores. In summary, the experiments presented here support the conclusion that four binding-competent subunits are required for IP_3-mediated channel activation and demonstrate the general utility of concatenated proteins to illuminate IP_3R biology.

Discussion

A question fundamental to understanding the activation of IP_3R is how the IP_3 binding event in the N-terminus of the IP_3R subunit is transmitted to the channel pore localized in the distant C-terminus (8, 10, 13, 35). Multiple intra- and intersubunit interactions revealed by biochemical and structural studies, including a current model generated from a cryo-EM structure of the entire IP_3R at 4.7 Å resolution (8-11, 36), are likely critical to coupling IP_3 binding to channel opening. Central to understanding how the interactions between various domains gate the channel is determining the obligatory stoichiometry of IP_3 binding necessary for channel activation. Here, we provide several lines of evidence from assaying IP_3R channel activity that indicate that IP_3R channels must bind four IP_3 molecules to initiate activation and Ca^{2+} release. First, an analysis of the relationship between IP_3 binding and unidirectional Ca^{2+} flux is consistent with the idea that IP_3R1 has to be nearly fully occupied before Ca^{2+} release is activated. Because Ca^{2+} release is not an “all-or-nothing” event, these data can be explained if the graded response to IP_3 is a consequence of mass action increasing the probability that all 4 monomers are concurrently IP_3-bound. Secondly, coexpression of wild-type and ligand-binding defective subunits in both HEK-3KO and DT40-3KO cells significantly attenuated the formation of functional channels as evidenced by an apparent dominant-negative effect of ligand-binding deficient subunits. Clearly, the most definitive approach implemented in this study is the use of concatenated constructs whereby a single polypeptide channel of any predefined composition can be fashioned and expressed in isolation.

Previously, we characterized the biochemical and biophysical properties of the IP_3Rs assembled from dimers of concatenated pairs of subunits expressed as a single polypeptide (32, 37). Here, we extended this approach to produce channels of defined composition from all 4 subunits expressed as a single concatenated polypeptide. No oligomerization of individual subunits is necessary to form functional channels with this construct. These channels assembled from concatenated dimers (32) or a single concatenated polypeptide of all four subunits had the same properties as wild-type channels in terms of IP_3 binding, Ca^{2+} release, the amplitude and frequency of evoked Ca^{2+} signals, and the increase in IP_3 sensitivity resulting from ATP and Ca^{2+}. Further validation presented here showed that the single-channel conductance and open probability under various conditions are like those of channels assembled from monomeric subunits. Moreover, channel open and closed times, characteristics of channel gating and thus the biophysical fingerprints of IP_3R were identical comparing monomeric, concatenated dimeric, or concatenated tetrameric IP_3R (as

summarized in Table 1 and table S2). These data indicated that linking the IP_3R subunits does not constrain the normal gating of the channel and established that the concatenation of subunits is a valid technique to interrogate IP_3R function. Indeed, the cryo-EM structure of IP_3R1 shows a close juxtaposition of N- and C-termini of the tetrameric channel, which may explain how the four subunits of this extremely large tetrameric complex can be linked without compromising channel structure and, thus, activity (11).

Taking advantage of this approach, we systematically demonstrated that channels with fewer than four competent ligand-binding sites do not form IP_3R capable of opening and initiating Ca^{2+} release. Initially, we examined the IP_3-induced activity of concatenated dimeric IP_3R1 with one wild-type and one ligand-binding deficient subunit. This construct is expected to form channels with two intact binding sites. The results of three complementary experimental approaches to monitor channel activity indicated that two IP_3 binding events are not sufficient for channel activation. This notion is, however, not consistent with a previous report that heterotetrameric channels assembled from $R1_Q$ and binding-competent subunits were partially functional, leading the authors to conclude that less than full occupancy by IP_3 was sufficient to gate IP_3R (10). Although differing experimental systems and measurements of activity were used in this study, an interpretation from our data is that Ca^{2+} release observed in the previous study may be a consequence of the substantial IP_3 binding and Ca^{2+} release activity retained by the $R1_Q$ subunit and thus does not necessarily provide definitive evidence of the stoichiometry of IP_3 binding. Notwithstanding this apparent discrepancy, the absence of any activity in a concatenated single polypeptide channel with three intact binding sites is again consistent with the concept that all four subunits must be bound to ligand to initiate Ca^{2+} release.

IP_3R activation is a complex process and involves binding of Ca^{2+}, IP_3, ATP, and perhaps many other factors, including protein association or dissociation, redox regulation, and phosphorylation status (3, 7, 38). IP_3 is obligate for channel opening and Ca^{2+} is also required for optimal channel activation, although the exact mechanism by which these two co-agonists interact is not well established (3, 12, 26). Current proposals suggest that following IP_3 binding, Ca^{2+}-regulatory sites can be engaged to enhance IP_3R open probability (3, 22). Our data are important in understanding the activation of IP_3R involved in the initial Ca^{2+} release at “trigger” zones (39). The initial IP_3-induced Ca^{2+}-release event occurs before local Ca^{2+} concentrations at the IP_3R have increased, thus the intracellular Ca^{2+} concentration near the IP_3R would likely be less than the threshold needed to regulate IP_3R activity. Our single-channel data obtained with a Ca^{2+} concentration mimicking cellular resting levels, together with the intact cell intracellular Ca^{2+} concentration measurements in cells that were stimulated with agonists that increase IP_3, revealed that full IP_3 engagement of the IP_3R is necessary for the initial activation. These data, are, therefore, consistent with the idea that upon stimulation there is no absolute requirement for Ca^{2+} concentrations to increase above the resting level to initially open the IP_3R. Nevertheless, following the initial activation, neighboring IP_3Rs will experience an increase in local Ca^{2+} concentration; therefore, it is possible that the IP_3 binding requirement is altered under these conditions. However, we found that in permeabilized-cell assays and single-channel recordings constructs with fewer than 4 intact binding sites were refractory to opening over a wide range of activating IP_3, Ca^{2+}, and ATP concentrations. Although many factors may

affect the kinetics of IP_3R channel opening following binding of four IP_3 molecules, we conclude that each of the four subunits must bind IP_3 for the channel to open. IP_3R activity can be modulated by a variety of factors not addressed in the current studies, including by binding partners and redox modification (7, 22, 38, 40, 41). In general, these events occur by allosteric regulation of the functional affinity for IP_3 and not by altering IP_3 binding directly. Thus, although our findings clearly show that all four subunits must be bound to IP_3 to trigger channel activity in the conditions tested, it remains possible that the stoichiometry of IP_3 activation of IP_3R may be altered in particular metabolic conditions or in the presence of binding partners.

Why have IP_3R evolved to require that each monomer is bound to IP_3 prior to activation? Intracellular Ca^{2+} is essential for almost all cellular processes but, paradoxically, has detrimental consequences if not fine-tuned to meet the cell's physiological needs. Thus, eukaryotic cells have evolved very intricate Ca^{2+}-signaling cascades with multiple layers of checks and balances to maintain strict control over intracellular Ca^{2+} concentrations. The requirement for maximum ligand occupancy for channel activation may ensure against unwarranted and potentially deleterious increases in intracellular Ca^{2+} (20).

Finally, the experimental approach used in this study can be extended to address many unanswered questions pertaining to IP_3R biology, including the investigation of other ligand or binding factor stoichiometries, such as ATP, Ca^{2+}, or calmodulin (7, 22). Similarly, an increasing number of IP_3R mutations have been identified in human diseases, many of which clinically manifest in heterozygous patients (14-17). We predict that the use of concatenated IP_3R with the defined expression of monomers will be the method of choice to examine the pathophysiological roles of IP_3R channels containing various combinations of wild-type and mutant subunits.

Material and Methods

Reagents

All reagents used for SDS-PAGE were from Bio-Rad. DNA T4 ligase and restriction enzymes were purchased from New England Biolabs. Dulbecco's modified Eagle's Medium (4.5g/L D-glucose), RPMI 1640 media, G418 sulfate, penicillin/streptomycin, chicken serum, and β-mercaptoethanol were obtained from Life Technologies. Fetal bovine serum was purchased from Gemini. Protein A/G agarose beads were purchased from Santa Cruz. Rabbit antibodies recognizing IP_3R1 (CT1) raised against the C-terminal 19 amino acids of rat IP_3R1 and rabbit antibodies recognizing IP_3R2 raised against amino acids 320-338 in mouse IP_3R2 were generated by Pocono Rabbit Farms and Laboratories (32, 42). Mouse monoclonal antibody against residues 22-230 of human IP_3R3 was from BD Transduction laboratories. Dylight™ 800CW secondary antibodies were from Thermo Scientific. Fura2-AM was from TEFLABS. All other chemicals were obtained from Sigma unless otherwise indicated.

Plasmid Construction

All constructs used in this study were based on rat IP_3R1 or mouse IP_3R2 cloned in pcDNA3.1. DNA modifications were made following QuikChange mutagenesis as described before (32). All PCR steps were carried out using *Pfu* Ultra II Hotstart 2X Master Mix (Agilent). Primers used in this study were synthesized by Integrated DNA Technologies and are listed in table S3. To generate IP_3R1-R265Q, F1 and R1 primers were used. To introduce K508Q and R511Q mutations into IP_3R1, a F2 and R2 were used. To make mCherry-IP_3R1 fusion protein, an Nhe I site was engineered immediately after the start codon in IP_3R1 using F3 and R3 primers. To subclone mCherry coding sequence from pmCherry-C1 (Clontech), an NheI site was introduced at the end of coding sequence of mCherry using primer pair F4 and R4. The modified pmCherry-C1 plasmid was digested with NheI and the NheI-NheI fragment flanking mCherry coding region was inserted into the NheI site engineered before IP_3R1 coding sequence. To add a FLAG tag to the C-terminus of IP_3R1, F5 and R5 were used. To mutate the ligand-binding domain IP_3R2, F6 and R6 were used to introduce R568Q and K569Q mutations. Finally, F7 and R7 primer pair was used to make $R2_{short}$. The coding sequences and desired DNA modifications were confirmed by sequencing. Concatenated IP_3R subunits were created as described before (32, 33). Briefly, to make a concatenated R1R1 or R2R2 dimer, the corresponding IP_3R cDNAs in pcDNA3.1(+) vector were modified to introduce unique restriction sites and extra nucleotides encoding the 7-amino-acid linker (QLNQLQT), and then two cDNAs coding for IP_3R subunits were ligated tail-to-head between the two arms of pJAZZ mamm linear vector based on coliphage N15 (Lucigen, Middleton, WI). The resulting construct encodes two IP_3R subunits conjugated with a 14-amino-acid linker. Similarly, concatenated tetrameric IP_3R1 was made by linking four subunits to form one reading frame encoding four IP_3R subunits with 14-amino-acid linkers separating one subunit from the next. The coding sequences and desired DNA modifications were confirmed by sequencing.

Cell Culture and Transfection

DT40-3KO cell line and HEK293 cells were maintained accordingly as described before (2, 32). DT40-3KO cells were transiently transfected as follows: 5 million cells were pelleted by centrifugation and washed once with phosphate-buffered saline (PBS, pH 7.3) and then electroporated with 5 μg of plasmid DNA using Amaxa cell nucleofector kit T (Lonza Laboratories). Cells were supplied with fresh complete RPMI media (RPMI 1640 media supplemented with 1% chicken serum, 10% fetal bovine serum, 100 units/ml penicillin, 100 μg/ml streptomycin) and allowed to recover for 24 h and then used for experiments. For the generation of stable cell lines, 24 h post-transfection, cells were plated in media containing 2 mg/ml G418 in five 96-well plates. After 10-14 days, Western blot analyses were used to screen G418-resistant clones for expression of the desired constructs. For HEK293 cell transfection, cells were transfected with cDNA constructs using lipofectamine2000 following the manufacturer's protocol. Cells were used for experiment 24-48 hrs after transfection. Cell lysates, SDS-PAGE, and coimmunoprecipitation were carried out as described before (42).

CRISPR-mediated Disruption of Human IP_3R Complements in HEK293 cells

Single guide RNA (sgRNA) target sites in human *ITPR1*, *ITPR2*, and *ITPR3* loci were identified using CRISPR.mit.edu (30). Oligonucleotides corresponding to these sgRNAs, designed so that they can be annealed and cloned into pX458 vector (Addgene) that was digested with BbsI, were synthesized by Integrated DNA Technology. The pX458 vector encodes Cas9 nuclease and enhanced green fluorescent protein (EGFP) (30). Becuase our preliminary experiments showed that simultaneously using two sgRNAs to target each IP_3R was more effective in disrupting IP_3R-encoding alleles, two sgRNAs were chosen targeting the third and fourth exons in *ITPR1* gene and the first and fourth exons in *ITPR2* and *ITPR3*. pX458-sgRNAs were transfected into HEK293 cells. 48 hours posttransfection, EGFP-expressing cells were sorted and grown as single cells in 96-well plates. After three weeks, clones were screened by Western blotting using IP_3R subtype-specific antibodies. Potential clones were genotyped as follows: Genomic DNA was isolated and amplified using a pair of primer flanking the CRISPR target site. Amplicons were cloned into pcDNA3.1 (+) and sequenced. 6 clones were sequenced and sequencing data indicate the introduction of indels (insertion or deletion) in both alleles.

IP_3 binding Assay

IP_3R constructs stably expressed in DT40-3KO cells were immunoprecipitated. The binding reaction consisted of 100 μl volume containing equal amounts of immunoprecipitated proteins, 2.5 nM tritiated IP_3 (^3H-IP_3) in the presence or absence of increasing concentrations of unlabeled IP_3. Tubes were incubated for 1 h at 4°C with mixing every 10 min. Beads were then centrifuged at 13000 × g, supernatants were removed, and 500 μl of 1% of SDS was added to each tube. After 12-24 h, liquid scintillation counting was used to measure bound radioactivity. Nonspecific binding was calculated as the amount of bound radioactivity in the presence of 50 μM unlabeled IP_3. Specific binding is determined by subtracting nonspecific binding obtained in parallel. All values were normalized to total specific binding obtained in the absence of unlabeled IP_3. The averages of normalized values from 3-4 experiments were used to generate best fits. For Fig. 2A and Fig. 8B, specific binding was divided by the corresponding densitometric values, obtained from parallel analyses of immunoblots of equivalent amount of corresponding immunoprecipitated protein. These values were then normalized to that of IP_3R1 (Fig. 2A) and R2R2 (Fig. 8B).

Single Cell Imaging

Cytosolic Ca^{2+} changes were measured as described previously (32). Briefly, DT40-3KO cells expressing the indicated IP_3R constructs were loaded in imaging buffer (137 mM NaCl, 0.56 mM MgCl2, 4.7 mM KCl, 10 mM HEPES, 5.5 mM glucose, 1.26 mM Ca^{2+}, 1 mM Na_2HPO_4 at pH 7.4) containing 2 μM Fura2-AM and were placed on a glass coverslip mounted in a Warner chamber for 20 min at 37°C. Experiments were performed at 37° C. TILLvisION software was used for image acquisition and analyses. Experiments were repeated at least three times.

Permeabilized Cell Assays

Permeabilized-cell assays were carried out to assess unidirectional Ca^{2+} flux as described before (43). Briefly, cells were washed once with imaging buffer and incubated with 20 μM Furaptra-AM at room temperature for 1 hr and then permeabilized using 40 μM β-escin. Intracellular Ca^{2+} stores were loaded by adding 0.650 mM $CaCl_2$, 1.4 mM $MgCl_2$, and 1.5 mM Mg-ATP to activate the endoplasmic reticulum-localized Ca^{2+}-ATPase SERCA. Upon loading, SERCA was disabled by removing $MgCl_2$. IP_3Rs were then activated by addition of the indicated concentration of IP_3 in the presence of 5 mM ATP. The data was fit to a single exponential function to determine the initial release rate.

Homology Modeling

A homology-based model was generated for $R1_{QQQ}$ using version 9.16 of Modeller (29) in default mode. As a template, we used an available crystal structure of the IP_3R1 N-terminal region in the absence of IP_3 (PDB ID: 3UJ4) (28). This structure is resolved to a higher resolution in this domain (3.0 Å) than the cryo-EM structure of the entire IP_3R1 (4.7 Å), and the amino-acid side chains are clearly resolved. Structural models were generated using UCSF Chimera (44) and Pymol (Schrodinger, Cambridge, MA).

Single IP_3R1 channel measurements in isolated DT40-3KO nuclei

Isolation of nuclei and on-nucleus patch clamping were described before (34). Single IP_3R channel potassium currents (i_k) were measured in the on-nucleus patch clamp configuration using PClamp 9 and an Axopatch 200B amplifier (Molecular Devices, Sunnydale, California). Pipette solution contained 140 mM KCl, 10 mM HEPES, with varying concentrations of IP_3, ATP, BAPTA, and free Ca^{2+}. Free concentrations of Ca^{2+} were calculated using Max Chelator freeware. Traces were consecutive 3 second sweeps recorded at −100 mV, sampled at 20 kHz, and filtered at 5 kHz. A minimum of 15 seconds of recordings was considered for data analyses. Pipette resistances were typically 20 MOhms and seal resistances were >5 GOhms.

Data Analysis

Single-channel openings were detected by half-threshold crossing criteria using the event detection protocol in Clampfit 9. We assumed that the number of channels in any particular cell is represented by the maximum number of discrete stacked events observed during the experiment. Even at low probability of opening (P_o), stacking events were evident. Only patches with 1 apparent channel were considered for analyses. P_o, unitary current (i_k), open and closed times, and burst analyses were calculated using Clampfit 9 and Origin 6 software (Origin Lab, Northampton, Massachusetts). All-points current amplitude histograms were generated from the current records and fitted with a normal Gaussian probability distribution function. The coefficient of determination (R^2) for every fit was > 0.95. The P_o was calculated using the multimodal distribution for the open and closed current levels. Channel dwell-time constants for the open and closed states were determined from exponential fits of all-points histograms of open and closed times. The threshold for an open event was set at 50% of the maximum open current and events shorter than 0.1 ms were ignored. A ‘burst’ was defined as a period of channel opening following a period of no channel activity that

was greater than five times the mean closed time within a burst. The slope conductances were determined from the linear fits of the current–voltage relationships with the equation:

$$g = i_k / (V - V_k)$$

Where g is unitary conductance, i_k is unitary current, V is voltage, and V_k is the reversal potential. Ca^{2+} dependency curves were fitted separately for activation and inhibition with the logistic equation:

$$Y = \left[(A_1 - A_2) / \left(1 + (X/X_0)^P \right) \right] + A_2$$

Supplementary Material

Refer to Web version on PubMed Central for supplementary material.

Acknowledgments

Funding:

This work was supported by the NIH through RO1 DE014756 and DE019245 (to DIY).

References

1. Berridge MJ, Lipp P, Bootman MD. The versatility and universality of calcium signalling. Nat Rev Mol Cell Biol. 2000; 1:11–21. [PubMed: 11413485]
2. Alzayady KJ, Sebe-Pedros A, Chandrasekhar R, Wang L, Ruiz-Trillo I, Yule DI. Tracing the Evolutionary History of Inositol, 1, 4, 5-Trisphosphate Receptor: Insights from Analyses of Capsaspora owczarzaki Ca2+ Release Channel Orthologs. Mol Biol Evol. 2015; 32:2236–2253. [PubMed: 25911230]
3. Foskett JK, White C, Cheung KH, Mak DO. Inositol trisphosphate receptor Ca2+ release channels. Physiol Rev. 2007; 87:593–658. [PubMed: 17429043]
4. Taylor CW, Genazzani AA, Morris SA. Expression of inositol trisphosphate receptors. Cell Calcium. 1999; 26:237–251. [PubMed: 10668562]
5. Bezprozvanny I. The inositol 1,4,5-trisphosphate receptors. Cell Calcium. 2005; 38:261–272. [PubMed: 16102823]
6. Uchida K, Miyauchi H, Furuichi T, Michikawa T, Mikoshiba K. Critical regions for activation gating of the inositol 1,4,5-trisphosphate receptor. J Biol Chem. 2003; 278:16551–16560. [PubMed: 12621039]
7. Yule DI, Betzenhauser MJ, Joseph SK. Linking structure to function: Recent lessons from inositol 1,4,5-trisphosphate receptor mutagenesis. Cell Calcium. 2010; 47:469–479. [PubMed: 20510450]
8. Yamazaki H, Chan J, Ikura M, Michikawa T, Mikoshiba K. Tyr-167/Trp-168 in type 1/3 inositol 1,4,5-trisphosphate receptor mediates functional coupling between ligand binding and channel opening. J Biol Chem. 2010; 285:36081–36091. [PubMed: 20813840]
9. Seo MD, Velamakanni S, Ishiyama N, Stathopulos PB, Rossi AM, Khan SA, Dale P, Li C, Ames JB, Ikura M, Taylor CW. Structural and functional conservation of key domains in InsP3 and ryanodine receptors. Nature. 2012; 483:108–112. [PubMed: 22286060]
10. Boehning D, Joseph SK. Direct association of ligand-binding and pore domains in homo- and heterotetrameric inositol 1,4,5-trisphosphate receptors. EMBO J. 2000; 19:5450–5459. [PubMed: 11032812]

11. Fan G, Baker ML, Wang Z, Baker MR, Sinyagovskiy PA, Chiu W, Ludtke SJ, Serysheva II. Gating machinery of InsPR channels revealed by electron cryomicroscopy. Nature. 2015
12. Taylor CW, Tovey SC. IP(3) receptors: toward understanding their activation. Cold Spring Harb Perspect Biol. 2010; 2:a004010. [PubMed: 20980441]
13. Serysheva II, Ludtke SJ. 3D Structure of IP(3) Receptor. Curr Top Membr. 2010; 66:171–189. [PubMed: 22353480]
14. Bezprozvanny I. Role of inositol 1,4,5-trisphosphate receptors in pathogenesis of Huntington's disease and spinocerebellar ataxias. Neurochem Res. 2011; 36:1186–1197. [PubMed: 21210219]
15. Klar J, Hisatsune C, Baig SM, Tariq M, Johansson AC, Rasool M, Malik NA, Ameur A, Sugiura K, Feuk L, Mikoshiba K, Dahl N. Abolished InsP3R2 function inhibits sweat secretion in both humans and mice. J Clin Invest. 2014; 124:4773–4780. [PubMed: 25329695]
16. Foskett JK. Inositol trisphosphate receptor Ca2+ release channels in neurological diseases. Pflugers Arch. 2010; 460:481–494. [PubMed: 20383523]
17. Huang L, Chardon JW, Carter MT, Friend KL, Dudding TE, Schwartzentruber J, Zou R, Schofield PW, Douglas S, Bulman DE, Boycott KM. Missense mutations in ITPR1 cause autosomal dominant congenital nonprogressive spinocerebellar ataxia. Orphanet J Rare Dis. 2012; 7:67. [PubMed: 22986007]
18. Iwai M, Tateishi Y, Hattori M, Mizutani A, Nakamura T, Futatsugi A, Inoue T, Furuichi T, Michikawa T, Mikoshiba K. Molecular cloning of mouse type 2 and type 3 inositol 1,4,5-trisphosphate receptors and identification of a novel type 2 receptor splice variant. J Biol Chem. 2005; 280:10305–10317. [PubMed: 15632133]
19. Iwai M, Michikawa T, Bosanac I, Ikura M, Mikoshiba K. Molecular basis of the isoform-specific ligand-binding affinity of inositol 1,4,5-trisphosphate receptors. J Biol Chem. 2007; 282:12755–12764. [PubMed: 17327232]
20. Marchant JS, Taylor CW. Cooperative activation of IP3 receptors by sequential binding of IP3 and Ca2+ safeguards against spontaneous activity. Curr Biol. 1997; 7:510–518. [PubMed: 9210378]
21. Meyer T, Holowka D, Stryer L. Highly cooperative opening of calcium channels by inositol 1,4,5-trisphosphate. Science. 1988; 240:653–656. [PubMed: 2452482]
22. Taylor CW, Laude AJ. IP3 receptors and their regulation by calmodulin and cytosolic Ca2+. Cell Calcium. 2002; 32:321–334. [PubMed: 12543092]
23. Dufour JF, Arias IM, Turner TJ. Inositol 1,4,5-trisphosphate and calcium regulate the calcium channel function of the hepatic inositol 1,4,5-trisphosphate receptor. J Biol Chem. 1997; 272:2675–2681. [PubMed: 9006903]
24. Taylor CW, Rahman T, Tovey SC, Dedos SG, Taylor EJ, Velamakanni S. IP3 receptors: some lessons from DT40 cells. Immunol Rev. 2009; 231:23–44. [PubMed: 19754888]
25. Sugawara H, Kurosaki M, Takata M, Kurosaki T. Genetic evidence for involvement of type 1, type 2 and type 3 inositol 1,4,5-trisphosphate receptors in signal transduction through the B-cell antigen receptor. EMBO J. 1997; 16:3078–3088. [PubMed: 9214625]
26. Yoshikawa F, Morita M, Monkawa T, Michikawa T, Furuichi T, Mikoshiba K. Mutational analysis of the ligand binding site of the inositol 1,4,5-trisphosphate receptor. J Biol Chem. 1996; 271:18277–18284. [PubMed: 8663526]
27. Alzayady KJ, Wojcikiewicz RJ. The role of Ca2+ in triggering inositol 1,4,5-trisphosphate receptor ubiquitination. Biochem J. 2005; 392:601–606. [PubMed: 16134970]
28. Seo MD, Velamakanni S, Ishiyama N, Stathopulos PB, Rossi AM, Khan SA, Dale P, Li C, Ames JB, Ikura M, Taylor CW. Structural and functional conservation of key domains in InsP(3) and ryanodine receptors. Nature. 2012; 483:108–112. [PubMed: 22286060]
29. Sali A, Blundell TL. Comparative protein modelling by satisfaction of spatial restraints. Journal of Molecular Biology. 1993; 234:779–815. [PubMed: 8254673]
30. Ran FA, Hsu PD, Wright J, Agarwala V, Scott DA, Zhang F. Genome engineering using the CRISPR-Cas9 system. Nat Protoc. 2013; 8:2281–2308. [PubMed: 24157548]
31. Joseph SK, Bokkala S, Boehning D, Zeigler S. Factors determining the composition of inositol trisphosphate receptor hetero-oligomers expressed in COS cells. J Biol Chem. 2000; 275:16084–16090. [PubMed: 10747920]

32. Alzayady KJ, Wagner LE 2nd, Chandrasekhar R, Monteagudo A, Godiska R, Tall GG, Joseph SK, Yule DI. Functional inositol 1,4,5-trisphosphate receptors assembled from concatenated homo- and heteromeric subunits. J Biol Chem. 2013; 288:29772–29784. [PubMed: 23955339]
33. Chandrasekhar R, Alzayady KJ, Wagner LE 2nd, Yule DI. Unique Regulatory Properties of Heterotetrameric Inositol 1,4,5-Trisphosphate Receptors Revealed by Studying Concatenated Receptor Constructs. J Biol Chem. 2016; 291:4846–4860. [PubMed: 26755721]
34. Wagner LE 2nd, Yule DI. Differential regulation of the InsP(3) receptor type-1 and -2 single channel properties by InsP(3), Ca(2)(+) and ATP. J Physiol. 2012; 590:3245–3259. [PubMed: 22547632]
35. Chan J, Yamazaki H, Ishiyama N, Seo MD, Mal TK, Michikawa T, Mikoshiba K, Ikura M. Structural studies of inositol 1,4,5-trisphosphate receptor: coupling ligand binding to channel gating. J Biol Chem. 2010; 285:36092–36099. [PubMed: 20843799]
36. Schug ZT, Joseph SK. The role of the S4-S5 linker and C-terminal tail in inositol 1,4,5-trisphosphate receptor function. J Biol Chem. 2006; 281:24431–24440. [PubMed: 16815846]
37. Chandrasekhar R, Alzayady KJ, Wagner LE 2nd, Yule DI. Unique Regulatory Properties of Heterotetrameric Inositol 1,4,5-trisphosphate Receptors Revealed by Studying Concatenated Receptor Constructs. J Biol Chem. 2016
38. Joseph SK. Role of thiols in the structure and function of inositol trisphosphate receptors. Curr Top Membr. 2010; 66:299–322. [PubMed: 22353485]
39. Yule DI, Ernst SA, Ohnishi H, Wojcikiewicz RJ. Evidence that zymogen granules are not a physiologically relevant calcium pool. Defining the distribution of inositol 1,4,5-trisphosphate receptors in pancreatic acinar cells. J Biol Chem. 1997; 272:9093–9098. [PubMed: 9083036]
40. Choe CU, Ehrlich BE. The inositol 1,4,5-trisphosphate receptor (IP3R) and its regulators: sometimes good and sometimes bad teamwork. Sci STKE. 2006; 2006:re15. [PubMed: 17132820]
41. Bansaghi S, Golenar T, Madesh M, Csordas G, RamachandraRao S, Sharma K, Yule DI, Joseph SK, Hajnoczky G. Isoform- and species-specific control of inositol 1,4,5-trisphosphate (IP3) receptors by reactive oxygen species. J Biol Chem. 2014; 289:8170–8181. [PubMed: 24469450]
42. Alzayady KJ, Chandrasekhar R, Yule DI. Fragmented inositol 1,4,5-trisphosphate receptors retain tetrameric architecture and form functional Ca2+ release channels. J Biol Chem. 2013; 288:11122–11134. [PubMed: 23479737]
43. Betzenhauser MJ, Wagner LE 2nd, Iwai M, Michikawa T, Mikoshiba K, Yule DI. ATP modulation of Ca2+ release by type-2 and type-3 inositol (1, 4, 5)-triphosphate receptors. Differing ATP sensitivities and molecular determinants of action. J Biol Chem. 2008; 283:21579–21587. [PubMed: 18505727]
44. Pettersen EF, Goddard TD, Huang CC, Couch GS, Greenblatt DM, Meng EC, Ferrin TE. UCSF Chimera--a visualization system for exploratory research and analysis. J Comput Chem. 2004; 25:1605–1612. [PubMed: 15264254]

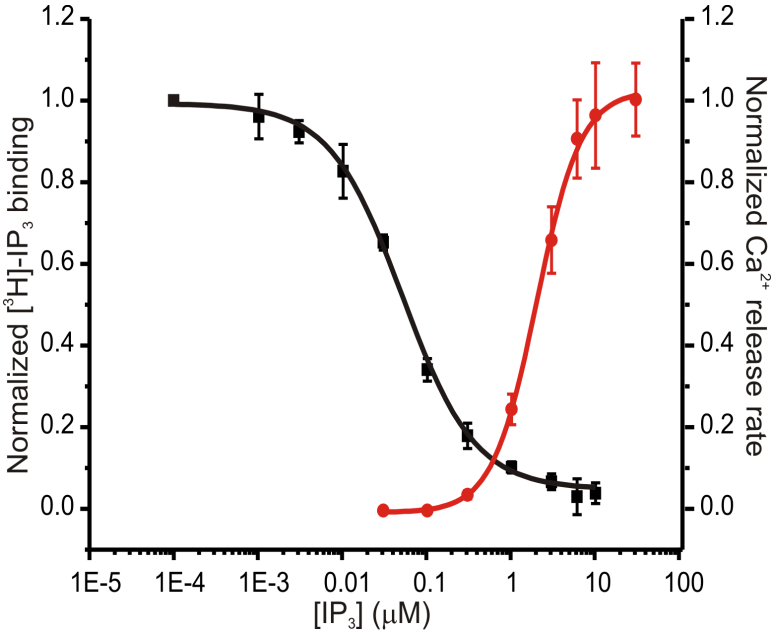

Figure 1. Comparing the IP_3 occupancy with IP_3-induced Ca^{2+} release in DT40-3KO cells expressing R1

Competitive binding assay was performed using IP_3R1 immunopurified from corresponding DT40-3KO cells. IP_3-evoked Ca^{2+} flux was assessed in permeabilized DT40-3KO cells expressing R1. Normalized values were plotted as a function of the log[IP_3]. EC_{50} for IP_3 binding is 50 nM ± 5 nM and EC_{50} for Ca^{2+} release is 1.84 μM ± 0.3 μM. Data are shown as mean ± SE of at least three independent experiments.

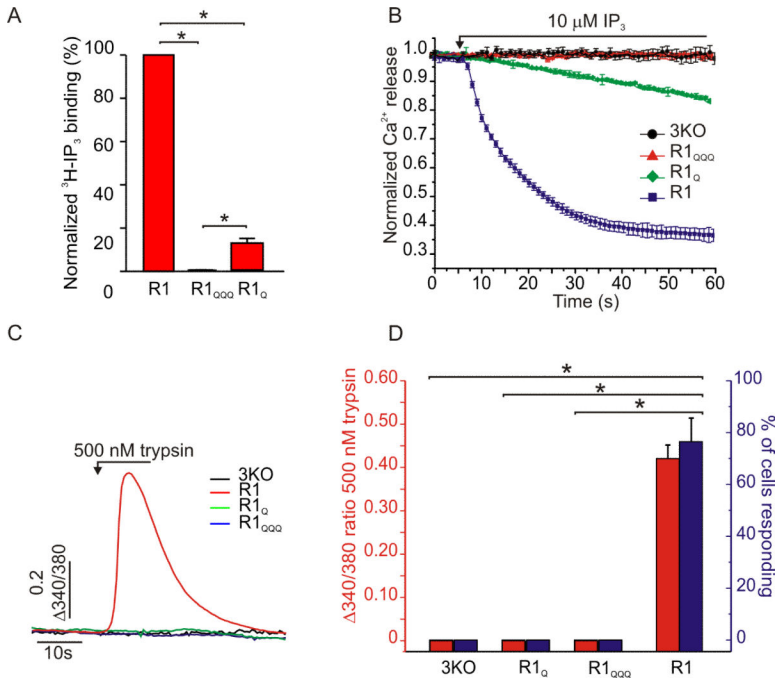

Figure 2. Evaluating the function of IP$_3$R1 with different mutations in the ligand-binding domain expressed in DT40-3KO cells

(**A**) DT40-3KO cells expressing the indicated IP$_3$R constructs were lysed and IP$_3$R proteins were immunoprecipitated and used for binding assays. Specific-binding values were divided by the amounts of the corresponding immunoprecipitated proteins and these values were normalized to that of the R1-expressing cells. Statistical analysis was carried out with one-way ANOVA followed by Tukey *post hoc* test. Pooled data from three independent experiments is shown. (**B**) Unidirectional Ca^{2+} flux assays in permeabilized DT40-3KO cells stably expressing the indicated IP$_3$R constructs and loaded with Furaptra. Data presented as mean ± SE of at least three experiments. (**C**) Trypsin-stimulated Ca^{2+} release in DT40-3KO cells stably expressing the indicated IP$_3$R constructs. The cells were loaded with Fura-2AM and stimulated with 500 nM trypsin. Representative traces are shown. (**D**) Quantitative analysis of the response of the indicated IP$_3$R-expressing DT40-3KO cells to trypsin. Red histograms depict the average maximum change over basal 340/380 fluorescence ratio resulting from trypsin stimulation. Blue histograms represent percentage of the cells responding to trypsin with >0.1 change in the 340/380 fluorescence ratio. Data are presented as mean ± SE. Experiments were repeated at least three times with more than 60 cells analyzed in each experiment. * denotes statistically significant differences (p<0.01) as determined by Tukey *post hoc* test.

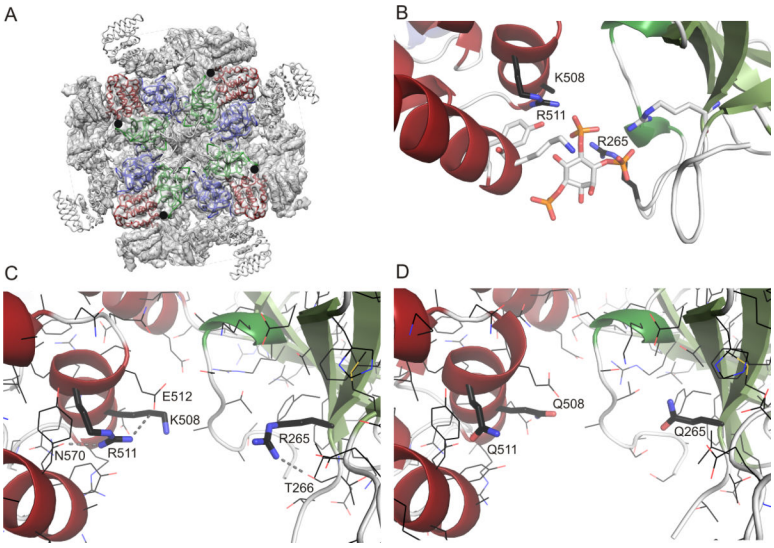

Figure 3. Overview of the IP_3R1 structure and IP_3 binding site

(**A**) Cryo-EM structure of type 1 IP_3R (cytosolic view), showing the electron density map in transparent white (EMDB entry 6369) (11), and the model in cartoon representation (PDB ID: 3JAV). The area for which crystal structures are available is highlighted in colors, with the suppressor domain in blue, and the two domains contributing to IP_3 binding in green and red. The structure was solved in the absence of IP_3, but its binding site in each subunit is indicated by black spheres. (**B**) Close-up of the 3.6Å crystal structure of the IP_3R N-terminal region in complex with IP_3 (PDB ID: 3UJ0) (28). The IP_3, as well as selected residues that make interactions, are shown in stick representation. The residues mutated in this study are indicated in black and labelled (numbering according to rat IP_3R1). (**C**) Close-up of the 3.0Å crystal structure of the IP_3R N-terminal region without IP_3 (PDB ID: 3UJ4) (28). All side chains are shown in black, with the three residues mutated in this study in stick representations. Hydrogen bonds made with the three residues are shown as dashed lines. Only the hydrogen bonds with R511 are observed in both molecules of the asymmetric unit. (**D**) Homology-based model of the $R1_{QQQ}$ mutant, showing the same area as in panel C.

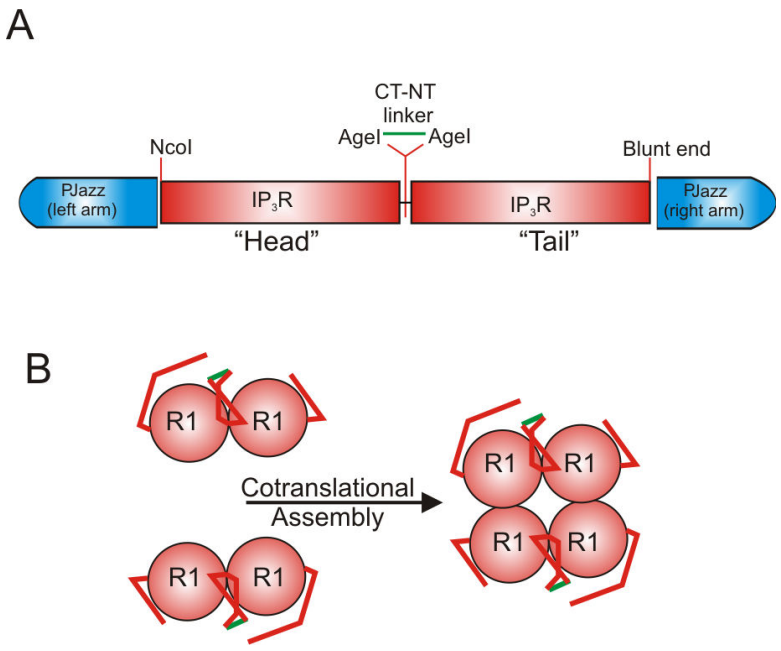

Figure 4. Attenuation of IP_3-induced Ca^{2+} signal in DT40-3KO cells and HEK-3KO expressing IP_3-binding deficient subunits

(**A**) Ca^{2+} release in transiently transfected cells loaded with Fura-2AM and stimulated with 50 nM trypsin. Inset, lysates from DT40-3KO cells expressing FLAG-tagged IP_3R1 transfected with mCherry or mCherry-tagged R1 (cherryR1) were mock-treated or immunoprecipitated with antibodies recognizing FLAG antibodies and immunoblotted for the indicated tags. (**B**) Quantitative analysis of the response of the indicated IP_3R-expressing DT40-3KO cells from A. Data presented as mean ± SE of at least four independent experiments. * denotes statistically significant differences ($p<0.01$). (**C**) Ca^{2+} release in transiently transfected HEK-3KO cells loaded with Fura-2AM and stimulated with 500 pM trypsin. Inset, lysates of HEK-3KO cells expressing the indicated constructs or vector-control cells were analyzed by immunoblotting for IP_3R1. (**D**) Quantitative analysis of the response of the indicated IP_3R-expressing cells from C. Data presented as mean ± SE of at least four independent experiments. * denotes statistically significant differences ($p<0.01$) as determined by Tukey *post hoc* test.

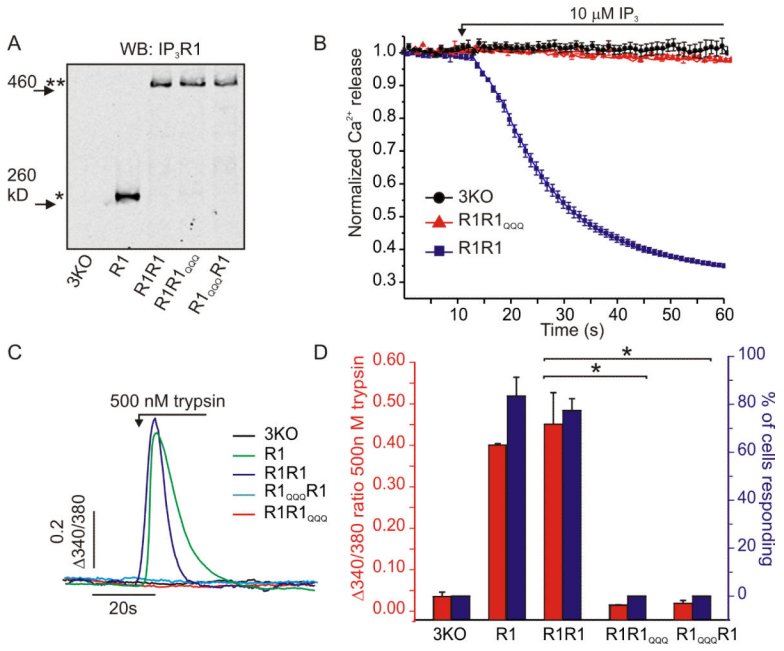

Figure 5. Diagram showing the construction of dimeric R1 and its oligomerization into a functional receptor

(**A**) A cartoon depicting a dimeric R1 cDNA construct flanked by the two arms of the linear vector, pJAZZ mamm. The “head subunit” (cDNA coding for rat IP_3R1_{QQQ}) was modified so that it contains an NcoI site just before the start codon. The stop codon was deleted and a nucleotide sequence coding for a 7-amino-acid-linker was added after the IP_3R1 coding sequence followed by an AgeI site. The “tail” subunit (cDNA coding for rat IP_3R1) was modified so that it contains an AgeI site followed by a nucleotide sequence coding for a 7 amino acid linker inserted before the start codon, and a blunt end restriction site was inserted after the stop codon. The resultant construct encodes one open reading frame consisting of two IP_3R subunits connected with a 14 amino acid linker. (**B**) A scheme showing how dimeric R1R1 molecules assemble to form a tetrameric channel.

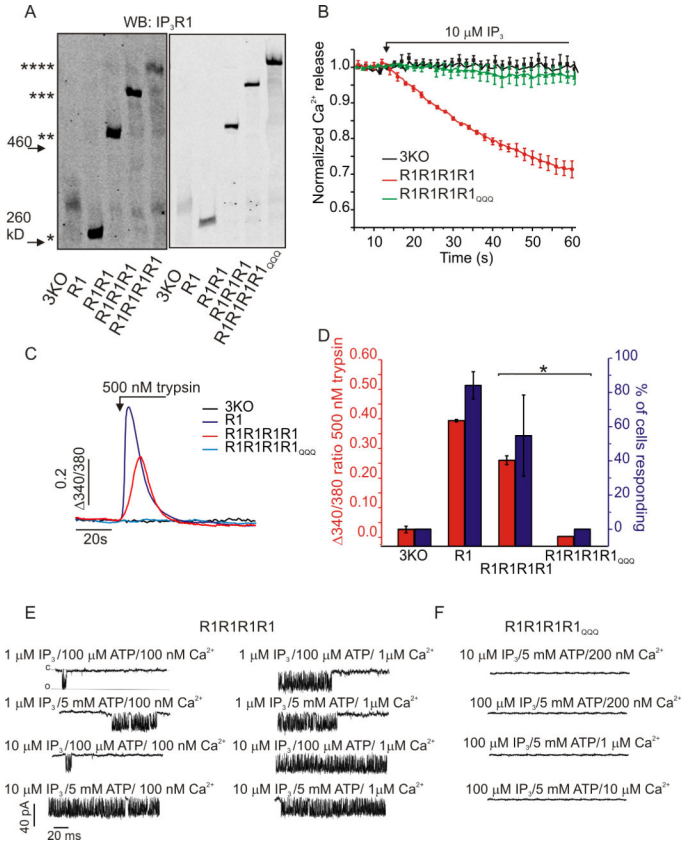

Figure 6. IP$_3$R channels with two ligand binding-deficient subunits are not functional

(**A**) Immunoblot shows the abundance of the indicated IP$_3$R constructs. The number of asterisks corresponds to the number of the concatenated subunits in the IP$_3$R1 constructs. (**B**) Unidirectional Ca^{2+} flux assays in permeabilized DT40-3KO cells stably expressing the indicated IP$_3$R constructs. Cells were loaded with Furaptra-AM and permeabilized, and Ca^{2+} flux was measured. Independent experiments were repeated at least three times in which greater than 60 cells were imaged in each experiment. Data presented as mean ± SE. (**C**) Trypsin-stimulated Ca^{2+} release in DT40-3KO or DT40-3KO cells stably expressing IP$_3$R constructs as indicated. Cells were loaded with Fura-2AM and stimulated with 500 nM trypsin. Representative traces are shown. (**D**) Quantitative analysis of the response of the indicated IP$_3$R-expressing DT40-3KO cells in C. Red histograms depict the average change over the basal 340/380 fluorescence ratio resulting from trypsin stimulation. Blue histograms represent percentage of the cells responding to trypsin with >0.1 change in the 340/380 fluorescence ratio. * denotes Tukey *post hoc* statistically significant differences ($p<0.01$).

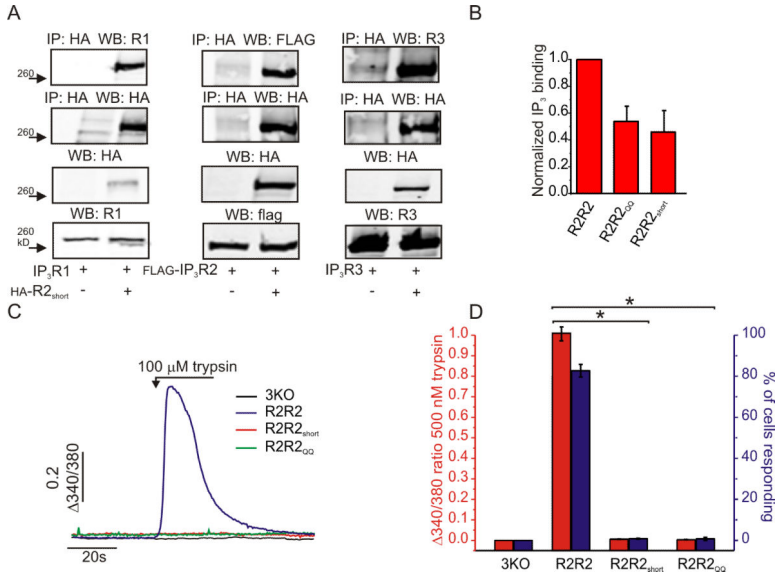

Figure 7. IP_3R channels with one ligand binding-deficient subunits are not functional

(**A**) Immunoblot shows the abundance of the indicated IP_3R constructs. The number of asterisks corresponds to the number of the concatenated subunits in the IP_3R1 constructs. (**B**) Unidirectional Ca^{2+} flux assays in permeabilized DT40-3KO cells stably expressing the indicated IP_3R constructs. Cells were loaded with Furaptra-AM and permeabilized, and Ca^{2+} flux was measured. Independent experiments were repeated at least three times. Data presented as mean ± SE. (**C**) Trypsin-stimulated Ca^{2+} release in DT40-3KO or DT40-3KO cells stably expressing IP_3R constructs as indicated. Cells were loaded with Fura-2AM and stimulated with 500 nM trypsin. Independent experiments were repeated at least three times where greater than 30 cells were imaged in each experiment. Shown are representative traces. (**D**) Quantitative analysis of the response of the indicated IP_3R-expressing DT40-3KO cells in C. Red histograms depict the average change over the basal 340/380 fluorescence ratio resulting from trypsin stimulation of corresponding cells. Blue histograms represent percentage of the cells responding to trypsin with >0.1 change in the 340/380 fluorescence ratio. * denotes statistically significant differences ($p<0.01$). (**E**) Single-channel recordings of DT40-3KO cells expressing the 4-concatenated subunit IP_3RI. Recordings were made with the “on-nucleus” configuration of the patch-clamp technique. Left traces show the effect of two concentrations of ATP on channel activity in response to a low (1 μM) and high (10 μM) concentration of IP_3. Right traces show effect of two concentrations of Ca^{2+} on channel activity in response to a low and high concentrations of IP_3. (**F**) Single-channel recordings of DT40-3KO cells expressing the 4-concatenated subunit lacking one ligand-binding site using the on-nucleus configuration. Recordings with two concentrations (10 μM and 100 μM) of IP_3 in the presence of 3 concentrations (200 nM, 1 μM, 10 μM) of Ca^{2+} are shown.

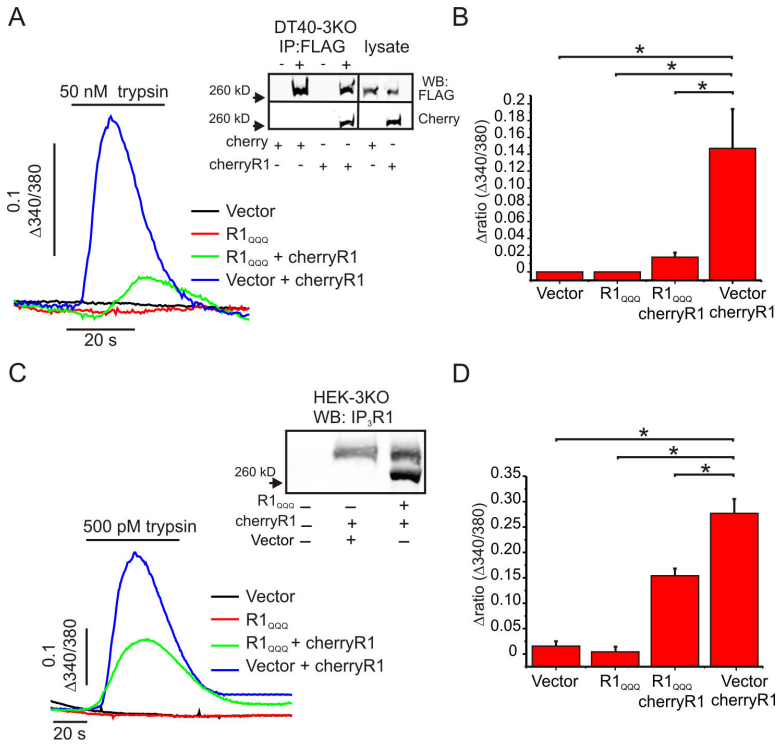

Figure 8. Assessment of $R2_{short}$ oligomerization, IP_3 binding, and Ca^{2+} release

(**A**) Immunoblot shows the abundance of the indicated IP_3R proteins from transiently cotransfected HEK293 cells. Lysate proteins were immunoprecipitated with the indicated antibodies and proteins were detected with antibodies recognizing the indicated protein or tag. Lower two panel depict lysate input. (**B**) IP_3 binding of the indicated dimeric constructs immunopurified from corresponding DT40-3KO cell lines. Binding values were divided by corresponding densitometric values obtained from parallel immunoblots and the results were normalized to that of R2R2. (**C**) Trypsin-stimulated Ca^{2+} release in DT40-3KO or DT40-3KO cells stably expressing IP_3R constructs as indicated. Cells were loaded with Fura-2AM and stimulated with 500 nM trypsin. Independent experiments were repeated at least three times where greater than 50 cells were imaged in each experiment. Shown are representative traces. (**D**) Quantitative analysis of the response of the indicated IP_3R-expressing DT40-3KO cells in C. Red histograms depict the average change over the basal 340/380 fluorescence ratio resulting from trypsin stimulation of corresponding cells. Blue histograms represent percentage of the cells responding to trypsin with >0.1 change in the 340/380 fluorescence ratio. *denotes statistically significant differences (p<0.0l) as determined by Tukey *post hoc* test.

Table 1

Biophysical properties of wild-type IP_3R formed from monomeric subunits, IP_3R formed from concatenated receptor subunit dimers, and single polypeptide IP_3R in response to maximal and submaximal IP_3.

10 μM IP_3, 5 mM ATP, 200 nM Ca^{2+}	**R1**	**R1R1**	**R1R1R1R1**
P_o	0.65 ± 0.05	0.7 ± 0.05	0.68 ± 0.05
Intraburst Mean Open Times	0.3 ± 0.01 ms	0.3 ± 0.01 ms	0.3 ± 0.01 ms
Intraburst Mean Closed Times	0.2 ± 0.02 ms	0.2 ± 0.02 ms	0.2 ± 0.02 ms
Burst Length	220 ± 9.8 ms	215 ± 9.7 ms	219 ± 10.1 ms
Interburst Interval	2.2 ± 0.5 ms	2.1 ± 0.5 ms	2.1 ± 0.5 ms

1 μM IP_3, 5 mM ATP, 200 nM Ca^{2+}	**R1**	**R1R1**	**R1R1R1R1**
P_o	0.28 ± 0.025	0.27 ± 0.024	0.275 ± 0.024
Intraburst Mean Open Times	0.3 ± 0.01 ms	0.3 ± 0.01 ms	0.3 ± 0.01 ms
Intraburst Mean Closed Times	0.2 ± 0.02 ms	0.2 ± 0.02 ms	0.2 ± 0.02 ms
Burst Length	94.9 ± 4.8 ms	94.7 ± 5.1 ms	95.1 ± 5 ms
Interburst Interval	14.2 ± 1.2 ms	14.5 ± 1.1 ms	14.3 ± 0.9 ms